Superelasticity and fatigue in oligocrystalline shape memory alloy microwires

Superelasticity and fatigue in oligocrystalline shape memory alloy microwires

Stian M. Ueland, Christopher A. Schuh[1]

Department of Materials Science and Engineering, Massachusetts Institute of Technology, 77 Massachusetts Avenue, Cambridge, MA 02139, USA

In oligocrystalline shape memory alloys, the total grain boundary area is smaller than the surface area of the specimen, leading to significant effects of free surfaces on the martensitic transformation and related shape memory and superelastic properties. Here we study sample size effects upon the superelastic characteristics of oligocrystalline microwires after one loading cycle and after many. Cu-Zn-Al wires with diameters ranging from ~100 down to ~20 μm are fabricated by the Taylor liquid processing technique and characterized through both uniaxial cyclic tensile testing and mechanically constrained thermal cycling. The energy dissipated per superelastic cycle increases with decreasing wire diameter, and this size effect is preserved after extensive cycling despite a significant transient evolution of the superelastic response for early cycles. We also present fatigue and fracture data indicating that oligocrystalline wires of this normally brittle alloy can exhibit fatigue lifetimes two orders of magnitude improved over conventional polycrystalline Cu-Zn-Al.

Keywords: Shape memory alloys; martensitic transformation; size effects; fatigue; cyclic loading

[1] Corresponding author. Email address: schuh@mit.edu (C.A Schuh).

1. Introduction

The diffusionless solid-state martensitic phase transformation in shape memory alloys (SMAs) gives rise to interesting and useful properties, such as the shape memory effect, the two-way memory effect and superelasticity [1-12]. Whereas shape memory is of interest in energy conversion and actuation, superelasticity is characterized by a hysteretic stress-strain response and is particularly interesting for applications in impact absorption and damping [13]. Of the many SMA families that have been reported in the literature, the Cu-based SMAs are attractive because they can exhibit excellent shape memory properties at a substantially lower materials cost relative to the market-dominant Ni-Ti-based alloys. On the other hand, the stress concentrations at grain boundaries and triple junctions that arise to maintain coherency of the transformation strains make the Cu-based SMAs prone to brittle intergranular fracture [14, 15]. This limits the utility of polycrystalline Cu-based SMAs to small shape memory strains and low numbers of cycles, and renders their shape forming in the solid state difficult or impossible. However, recent progress on Cu-based SMAs in structures where grains are less constrained has pointed towards a strategy to overcome the problems associated with grain boundary fracture.

Through microstructural design and the formation of an "oligocrystalline" structure, the constraints of the polycrystalline structure upon the martensitic transformation can be reduced to a point that single crystal-like SMA properties are possible without fracture [16]. An oligocrystalline structure can be defined as one where the total surface area is greater than the total grain boundary area, meaning that grains are coordinated mostly by unconfined free surfaces rather than rigid boundaries with other grains. The oligocrystalline structures that have been studied to date in conventional SMAs are based on fine wires with a bamboo grain structure [16-18], with some preliminary work on open-cell foams [19, 20]; the same concept has been explored in magnetic SMA foams at an even earlier date [21].

The production of an oligocrystalline structure generally requires significant reduction of one or more of the sample dimensions. The study of oligocrystalline SMAs therefore is naturally associated with the exploration of sample size effects upon the martensitic phase transformation and shape memory properties. In the work of Chen and Schuh [17], the hysteresis of a superelastic cycle was found to increase dramatically as the diameter of bamboo structure wires was reduced from ~100 to ~20 μm. This result aligns well with a previously-reported sample size effect on single crystal Cu-Al-Ni submicron pillars, for which San Juan et al. [22, 23] reported energy dissipation much higher than is seen in bulk single crystals. Chen and Schuh analyzed the various possible physical origins of this effect, and concluded that free surfaces enhanced the internal frictional work associated with moving the martensite/austenite phase boundaries [17]. Based on this insight, a nonlocal continuum-mechanical model was developed by Qiao et al. [24] and was able to reproduce the size-dependence of superelastic stress-strain curves in micropillars.

The above works on oligocrystalline SMAs are very few, and there remain many outstanding questions that need to be addressed before their true application potential can be evaluated. For example, to date the only systematic work has been on a single alloy (Cu-Al-Ni), and the generality of both sample size effects on damping, as well as the proposal that the oligocrystalline structure can alleviate the intergranular fracture problem of polycrystals, have yet to be verified in any other SMA. Additionally, there is as yet no data to suggest that the oligocrystalline structure can lead to stable shape memory and superelastic properties over many transformation cycles such as are required in SMA applications. Lastly, the tendency to fracture along grain boundaries makes fatigue in Cu-based SMAs inherently linked to microstructure. While single crystals can exhibit good fatigue behavior [25], this is disappointingly not the case for polycrystals [26]. In light of its good superelastic properties it is therefore interesting to see whether the oligocrystalline structure can approach single crystal fatigue life or at least achieve values comparable to commercial Ni-Ti [27].

The purpose of this paper is to address these issues. We prepare oligocrystalline fibers of a second Cu-based SMA (Cu-Zn-Al), and validate the proposal of Chen et al. [16] that this microstructural form is indeed capable of full superelastic and shape memory behavior without suffering early intergranular fracture. We also verify the size effect seen in prior works, whereby smaller diameter fibers damp more energy during a full transformation cycle. Finally, we present the first exploration of cyclic loading and fatigue failure in oligocrystalline SMAs, and validate that acceptable low-cycle fatigue properties are possible in this new class of alloys.

2. Material production and characterization

Oligocrystalline SMA fibers were prepared using the Taylor liquid drawing technique [28, 29] following the first report of Chen et al. [16] in the Cu-Al-Ni system. Solid pieces of alloy with composition Cu-22.9%Zn-6.3%Al (wt.%) were placed in a closed-end aluminosilicate glass tube with 4 mm inner diameter and a working temperature of ~1250 ºC. The inside of the tube was then subjected to low vacuum conditions and heated by an oxy-acetylene burner until the metal melted and the glass softened, at which point a glass capillary was drawn with the molten metal at its core. By varying the drawing speed we were able to produce wires with diameters ranging from ~20 to ~100 μm.

To promote grain growth into the stable bamboo structure, the as-drawn wires (still in the glass sheath) were annealed in an argon atmosphere for 3 h at 800ºC and water quenched. The glass coating was removed by immersion in ~10% diluted aqueous hydrofluoric acid. Finally, each fiber was left for a minimum of seven days at room temperature before being used in further experiments.

Fig. 1a shows a montaged optical micrograph of a typical fiber longitudinal cross section that was polished and etched in 50% diluted nitric acid. The wire exhibits a bamboo type structure where individual grains span the entire cross section and where grain boundaries are almost perpendicular to the fiber axis. This particular wire is observed in a duplex condition (below the austenite finish temperature A_f), and martensite plates spanning the entire cross section are therefore also visible, another signature of the oligocrystalline structure.

Figs. 1b-d show transverse cross sections of three different wires, illustrating the variety of cross-sections that are produced using our synthesis approach; one of these wires (b) exhibits a roughly equiaxed cross-section while the others (c-d) exhibit more irregular shapes. Because of these geometrical differences scanning electron microscopy (SEM) was used to calculate the circular equivalent diameter, D, based on the cross-sectional area of each wire. Other geometrical features, such as the shortest axis, the longest axis and the perimeter were also measured in this way. Table 1 lists all of the test specimens used in this work, labeled according to their equivalent diameter in descending order.

3. Mechanical testing and transformation characterization

Mechanical testing, including shape memory, superelasticity, and fatigue testing, was performed in the as-prepared condition following the removal of the glass sheath, without any additional surface treatment. Testing was conducted in tension under load-control using a dynamical mechanical analyzer equipped with a closed furnace (DMA Q800 from TA instruments). Each end of the wire was mounted in a plastic compound to form sound mechanical grips which were then clamped. The cross-head displacement was measured by a high resolution linear optical encoder within the instrument, with a nominal resolution of 1 nm. The gauge length varied between 2 - 5 mm for different wires.

Constrained thermal cycling was performed on sample #2 (D = 61 μm) in order to reveal the stress-assisted two-way shape memory effect and to identify the transformation temperatures. This was done by applying a small preload (0.01 to 0.05 N, amounting to a stress level of 3 to 17 MPa) and thermally cycling at a rate of 2 ºC/min. As shown in Fig. 2, elongation is recorded when transforming to martensite upon cooling and contraction upon reversion to austenite during heating. The transformation strain is completely recovered and the maximum strain increases from 4.5 to 6.4 % when the applied stress is increased from 3 to 17 MPa. The thermal hysteresis is ~18 ºC and the transformation temperatures are seen to increase with increasing load as described by the Clausius-Clapeyron equation.

By calculating M_s for each thermal cycle at different applied stresses (3, 10 and 17 MPa) we obtain a linear relation between temperature and stress, $\sigma_{a\to m} = 2.3(T + 275)$, where $\sigma_{a\to m}$ is the stress to induce martensite in MPa and T is the temperature in Kelvins. The value 2.3 $MPa \cdot K^{-1}$ is the slope of the Clausius-Clapeyron equation, and is consistent with prior values reported for similar alloys, e.g., 2.1 by Saburi et al. [30] and 2.35 by Chandrasekaran et al. [31]. Similar relations were obtained for A_f, A_s and M_f, and by extrapolating to a condition of zero applied stress the characteristic transformation temperatures for sample #2 are obtained: M_s = -2 , M_f = -10 , A_s = 9 and A_f = 15 ºC. Furthermore, the Clapeyron slope for the austenite finish temperature (2.8 $MPa \cdot K^{-1}$) obtained from sample #2 is used to calculate A_f for each wire in Table 1 by extrapolating from the end of the reverse transformation to a condition of zero stress. This analysis accounts for differences in A_f among the wires due to, e.g., size effects [17] and possibly from minor compositional variations as well.

All subsequent tests were performed under isothermal conditions above A_f in the following way. The first five cycles were performed by cycling between the unloaded state and a maximum load, σ_{max}, at a slow loading rate (generally around 20 MPa·min^{-1}, see Table 1). Then the wire was cycled at the same stress levels, but at a faster rate (generally around 200 MPa·min^{-1}, see Table 1) until fatigue failure, interrupted occasionally by a few cycles conducted at the slower rate in order to acquire high quality data for energy analysis. For the evaluation of superelastic characteristics (other than fatigue) curves obtained with the slow loading rate was used in order to avoid latent heat effects [17]. The exceptions from this are sample #2 and sample #11 which were only cycled at the fast rate, sample #1, sample #6 and sample #9 which were only cycled at the slow rate and sample #4 which was cycled at increasing stress amplitudes for the first five cycles; many of these details are compiled in Table 1. For all wires other than sample #2, care was taken so that no prior deformation or thermal cycling was conducted prior to superelastic cycling.

The strain amplitude was found to vary slightly (usually decrease) with cycling, but after a few dozen cycles settling into a constant value. After fatigue failure the fracture surface was examined by SEM. The test temperature, transformation stress for the first loading cycle, slow and fast loading rates as well as the stress and strain amplitudes for the fatigue tests are reported in Table 1 along with the number of cycles to failure N_f.

4. Superelasticity and cycling effects

4.1 Strain history dependence of superelasticity

Fig. 3 shows the true stress-true strain curve for sample #4 loaded in tension at increasing applied load levels, at a temperature of 50 ºC. The wire exhibits near perfect superelasticity with only a small accumulation of residual strain of 0.15% after 5 cycles. In bulk polycrystalline Cu-Zn-Al the largest reported reversible strain amplitude is only ~2% [32, 33] with further straining being accompanied by large residual strains [15]. In contrast, the present oligocrystalline wire can be deformed reversibly to more than 6% strain because of its particular grain structure, where triple junctions are absent, the number density of grain boundaries is reduced, and transformation stresses can be relieved at free surfaces, effectively reducing transformation incompatibilities.

Both the stress to induce martensite $\sigma_{a\rightarrow m}$ and the reverse transformation stress $\sigma_{m\rightarrow a}$ are observed to decrease with continued cycling of the applied load, and this change is most pronounced between the first and second cycles. In fact, there is an interesting pattern of stress evolution from one cycle to the next: the forward transformation occurs at a lower stress plateau than for the preceding cycle, but only over the strain range of the previous cycle. Once the maximum strain of the previous cycle is reached, and the sample is experiencing higher strains for the first time, the forward transformation stress plateau increases to match the level of the preceding cycle. At this point the stress-strain curve continues from where the previous cycle left off, as though the preceding cycle had never been interrupted.

A similar effect has been reported in ultra-fine grained Ni-Ti SMAs by Yawny et al. [34], who attributed it to substructure development. Dislocations introduced to accommodate martensite plates in the austenite matrix during the first loading cycle [35] create an easy path that favorably oriented plates can grow into, and possibly also provide sites for plate nucleation [36], such that on subsequent reloading the substructure assists the development of the same martensite domains at lower stresses. Yawny et al. [34] presented data for polycrystalline samples, but noted that the same explanation applies to single crystals. In principle, the internal stress fields created this way can also explain the lowering of the reverse transformation plateau seen in Fig. 3. The shakedown of the lower plateau is less pronounced than that of the upper plateau, and this also aligns with data for ultrafine grained Ni-Ti [34].

4.2 Cyclic evolution of hysteresis

The cyclic shakedown of the transformation stresses seen in Fig. 3 is generally observed in all of our specimens, and because the upper plateau is more affected by cycling than is the lower one, the hysteresis decreases upon cyclic loading. In order to study this evolution more systematically, we conducted experiments involving cyclic loading at a constant stress amplitude (rather than an increasing one as in Fig. 4), and also explicitly considered a range of wire diameters.

Fig. 4 presents true stress-true strain curves of the 1st, 10th and 300th cycle of sample #10. The wire is previously undeformed and the stress step in the first curve is likely caused by the favorable orientation of one of the grains or by local non-uniformity in diameter and not by previous deformation. It is encouraging that only little residual strain is accumulated even after extensive cycling. Furthermore, in line with the prior results in Fig. 3, we notice that $\sigma_{a\to m}$ decreases dramatically while $\sigma_{m\to a}$ is almost unaltered and hence the hysteresis width is reduced. It is also interesting to note that ε_{max} is unchanged, despite testing being performed in load control to constant σ_{max}. This is a general trend observed for all the wires regardless of ε_{max} and should not be taken as an indication that the entire wire is completely transformed to martensite. Rather, as shown in Fig. 3, the stress will have to exceed σ_{max} in order for non-transforming parts of the wire to transform to martensite. Lastly, we note that the transformation slopes are similar for all cycles, except at the very end of the plateau as the transformation becomes exhausted and the curve steepens. No recovery was observed when this wire was aged at the test temperature for 24 h between cycle number 300 and 301.

The most striking consequence of repeated cycling is the reduction of the area inside the superelastic loop, i.e., the hysteresis energy dissipated per unit volume ΔE. In order to compare the dissipated energy across samples tested to different strains and at different temperatures, we use the strain-amplitude normalized quantity introduced by Chen and Schuh [17], the characteristic energy dissipation per volume per unit strain $\Delta E_{1\%}^{N}$, to which we add the superscript N to denote cycle number.

The evolution of $\Delta E_{1\%}^{N}/\Delta E_{1\%}^{1}$with cycling is shown in Fig. 5 for three wires with different diameters. In all our experiments the energy dissipation is observed to change with cycling in the same way: the decrease is dramatic for the first few cycles—the energy dissipation capability of these wires is reduced by ~40% after only ~5 cycles—with subsequent cycling resulting in only gradual additional reduction in $\Delta E_{1\%}$, e.g., for the wire shown in Fig. 4 the value of $\Delta E_{1\%}^{300}/\Delta E_{1\%}^{1}$ is reduced to 0.33. The similarity amongst the datasets in Fig. 4 suggests that this evolution in $\Delta E_{1\%}$ does not depend on wire size, at least over the studied range of D ≈ 20-120 µm. Note that this is a relevant range over which size effects do occur in oligocrystalline SMAs [17, 21] (which will be discussed at more length in the next section); these data show, however, that there is not a pronounced size effect on the shakedown behavior.

An evolution of energy dissipation similar to Fig. 5 has been found in some SMAs under different physical conditions, for example, when a non-transforming second phase has been introduced in Cu-Zn-Al single crystals [37-39], or in polycrystalline Ni-Ti [40-44]. In these studies, steady-state energy dissipation was found to develop after ~5-40 cycles [37, 38, 42-44] which agrees well with Fig. 5. The reason for the initial transient in the superelastic response in those works was attributed to microstructural changes such as the gradual generation of dislocations [37, 39-41], or development of stable areas of retained martensite

[38], all attenuating the additional pinning force of obstacles to the transformation. Such interpretations are supported by several recent studies focusing on the subtle microstructural changes caused by the formation of martensite in the austenite matrix [35, 45, 46]. Significant microplastic deformation and/or retained martensite are both considered somewhat unlikely in the case of present microwires; the tests are conducted well above A_f, so in every cycle the transformation strain was completely recovered, while residual stresses should be effectively relieved at free surfaces. Nonetheless, the similarity between the above studies and our results in Fig. 6 suggests some substructure development takes place, effectively reducing the pinning force on interface propagation during cycling. In microwires, it is possible that the structure evolution is related to the surface, where the most important obstacles to the transformation are believed to reside [17], although further work is needed to explore this possibility.

5. Size effects

Although the shakedown of the transformation stresses and hysteresis is common to all of our specimens and does not seem to change with sample size, a size dependence on the magnitude of the damping itself is recognized when the vertical axis in Fig. 6 is replaced by $\Delta E_{1\%}$ for the same three wires. This is shown in Fig. 6. Firstly, the initial value $\Delta E_{1\%}^{1}$ is observed to depend on wire diameter: the smaller the diameter, the larger the energy dissipation. In fact, $\Delta E_{1\%}^{1}$ for the smallest wire with D = 24 μm is 4-5 times larger than that for the largest wire with D = 113 μm. Secondly, as the samples all exhibit the same fractional attenuation of $\Delta E_{1\%}$ upon cycling (Fig. 5), the relative differences between them are conserved and the size effect is still present after 50 cycles (Fig. 6). Prior studies on bulk polycrystalline SMAs have revealed a grain size effect to appear on the same size scale (below ~100 μm) as the equivalent diameters used in the present study [47-50]. Furthermore, in the case of Cu-Al-Ni microwires [17], the stress hysteresis of the smallest wires (~20 μm) was reported to be ~3-7 times higher than that for the largest wires (~100 μm) which is similar in magnitude to Fig. 5 both before and after cycling.

To investigate the size effect in more detail the values of $\Delta E_{1\%}$ for the 1st and 50th cycles were recorded for twelve specimens and plotted against equivalent wire diameter in Fig. 7a. These data show that $\Delta E_{1\%}$ increases with decreasing diameter for the uncycled specimens, as well as after substantial cycling as suggested by Fig. 6. The dotted line in Fig. 8a represents a power-law fit of the form $\Delta E_{1\%} \propto D^{\alpha}$ where D is the wire equivalent diameter and the exponent α is found to be about 0.80 for the 1st cycle and about 0.75 for the 50th. The values of $\Delta E_{1\%}^{1}$ and $\Delta E_{1\%}^{50}$ are summarized in Table 1, along with $\Delta E_{1\%}^{1}/E_{max}$ for all of the wires.

The origin of the size effect on hysteresis in Fig. 7a has been attributed to frictional work spent on interface motion during transformations [17]. Because of the oligocrystalline geometry, martensite plates are envisioned to span the wire diameter (cf. Fig. 1), and the transformation propagates primarily by the thickening of these plates; the smaller the wire diameter, the stronger the pinning effect of surfaces on the phase boundaries as these plates thicken, degrading more mechanical energy into frictional work which is eventually dissipated in the form of heat [17]. The fact that the trend is similar for uncycled specimens and after 50 cycles suggests that the size effect originates from an intrinsic length-scale characteristic of the martensitic transformation and not from any particular microstructural features.

Although the superelastic response evolves with cycling, the dependence of energy dissipation on wire diameter appears relatively stable. In comparison to our sample size exponent of $\alpha \approx 0.7$-0.8, Chen and Schuh [17] found $\alpha \approx 0.54$ for Cu-Al-Ni wires in a range including wires with larger diameters than in the present study. When only wires with diameters between 23 and 109 μm were included, their power-law fitting yielded an exponent of α ≈ 0.66, which agrees reasonably with our result in Fig. 7. Any discrepancy may also be associated with subtle details of the wire shape. For a perfectly cylindrically shaped specimen, the diameter adequately reflects the decrease in the cross-sectional dimensions as well as the reduction in volume to surface ratio. However, the present wires occasionally have irregular cross-sections (cf. Fig. 1), so the equivalent diameter is no longer the only characteristic length that may affect the martensitic phase transformation. The major and minor cross-sectional axes (taken to be mutually perpendicular) of the wire are obvious candidate lengths, as is the volume-to-surface ratio parameter $L = 4V/A$, where V is the wire volume and A is the surface area. As previously done for the equivalent diameter D, a power law of the type $\Delta E_{1\%} \propto \mathrm{X}^{\alpha}$ is calculated for each of these characteristic lengths (X) and the results are reported in Table 2. It is interesting to note that the fit is improved (as measured by increase in the coefficient of determination, R^2) when the minor axis, which is the shortest cross-sectional dimension of the fiber, is used as the scaling parameter; this is plotted in Fig. 7b. What is more, the exponent of α ≈ 0.6-0.7 is closer to the value reported by Chen and Schuh [17] for Cu-Al-Ni. There is also a slight improvement for L for the first cycle, but this parameter is somewhat coupled with the shortest axis; a decrease in L at constant equivalent diameter is only possible if the wire assumes a more irregular shape, extending one axis at the expense of the other. The fit when using the longest axis is very poor.

Following this somewhat indirect indication that the sample size effect may scale with the shortest sample dimension, it is interesting to note that the thermally induced mean plate width in Cu-Zn-Al has been reported to be 35 μm after 1 cycle and decrease to 10 μm after 200 cycles [51]. These values are in the lower end of our equivalent diameter range and are better captured by the range of shortest axis. Additionally, a reduction of plate size with cycling may also help explain the apparent decrease in α with cycling; the characteristic length scale of martensite domains may decrease while the sample geometry is unchanging, permitting a dynamical cross-over in these scales.

6. Low Cycle Fatigue

6.1 Fatigue life

Since fatigue traditionally has been a weak point for many Cu-based SMA polycrystals, it is of obvious interest to explore larger numbers of superelastic cycles to ascertain whether the oligocrystalline structure offers a solution to this problem. Eleven of our specimens were cycled until failure under pure tensile loading (load ratio $R \approx 0$). The fatigue life data for these samples are presented in Fig. 8, as the number of cycles to failure, N_f, against strain amplitude.

Although the number of samples tested here is small, the data are reasonably clustered and fatigue life appears to be roughly independent of strain amplitude in the range 3.2-7.5%. The lack of strain amplitude dependence may be partly related to the fact that the stress amplitude is different from sample to sample. However, a plot of σ_{max} against N_f (not shown) yields even more scatter, and is less relevant for comparison with literature data because such studies have often involved single phase austenite, single phase martensite as well as dual phase cycling concomitantly. The strain amplitude independence is more likely explained by the heterogenous manner in which the transformation proceeds. In SMAs, deformation involving the movement of austenite/martensite interfaces is thought to have the worst effect on fatigue life [52], and it can therefore be expected that failure will eventually occur in a heavily transformed region. For incomplete transformations in a bamboo structure wire, some favorably oriented or seeded parts of the wire may undergo the complete martensitic transformation while other parts could transform incompletely, or even remain in the austenite phase during the whole experiment. Those parts of the wire that undergo the most detrimental movement of the austenite/martensite interface will ultimately be the location of failure, while the remaining parts will not appreciably contribute to fatigue life. Following this line of reasoning, the only difference between large and small strain amplitudes would be the volume fraction of wire transforming, and thus the fatigue life can be relatively independent of strain amplitude. This result has interesting consequences for use of oligocrystalline SMAs, which may be controlled by such weakest-link physics for many other properties as well. Clearly, improvements in fatigue lifetime under this scenario will be achieved by developing preferred textures without "weak orientations", or by removing potential transformation seeds.

In the same way as wire geometry was shown to influence size effects, shape and surface roughness may also be expected to affect fatigue life [53, 54]. In the present study, the surface finish is generally very rough and sharp corners where cracks can nucleate are present in many samples. Improved surface quality may therefore further improve the characteristics of oligocrystalline wires, but is left for future research.

Finally, it is useful to compare the present data with those for other SMAs; data for Ni-Ti [27, 55] (tested in rotating-bend mode with R = -1), Cu-Zn-Al polycrystals [26] (tested in tension-compression with R ~ -1) and Cu-Zn-Al single crystals [25] are also shown in Fig 9. In cases where different samples are tested we reproduce the sample which best matches our testing conditions, i.e., T_{exp} and A_f. The study on single crystal fatigue by Sade et al. [25] includes 44 different samples, all cycled to ~5% strain in pure tension, but to different stresses and temperatures. In Fig. 8 some representative results from the work of Sade et al. are plotted (their samples tested at room temperature and for which $M_s = 0$ºC).

There are several striking results that emerge from the comparison of the present data with these literature studies in Fig. 8. First, we note that the oligocrystalline structure offers a vast improvement in fatigue life in Cu-Zn-Al relative to polycrystals of the same alloy. This is especially true at large strain amplitudes (ε > 4%) where there is an improvement of more than two orders of magnitude compared to polycrystalline Cu-Zn-Al as reported by Melton and Mercier [26]. While the oligocrystalline samples still exhibit a fatigue deficit relative to the best single crystals of similar composition, they also seem to outperform at least some of the single crystal samples tested by Sade et al. [25]. The data here therefore illustrate the great potential of the oligocrystalline architecture, as a general microstructural engineering approach, to develop a compromise between production cost and properties in SMAs. Since polycrystalline Cu-Zn-Al has not usually been considered as a viable candidate material for actuator applications because of its tendency to fail when subjected to large actuation strains, the oligocrystalline form of the alloy exhibits significant enabling potential. This is especially true in light of the second comparison, namely, that the specific low-cycle fatigue lifetimes we present are comparable to Ni-Ti in the same strain range. This is very encouraging for possible low-cost substitution of oligocrystalline Cu-based SMAs for Ni-Ti in cyclic actuator applications, as Ni-Ti is the only alloy family with significant market traction in such applications.

6.2 Fatigue Fracture

The fatigue failure of structures with nominal bamboo grain structures is an interesting topic, though it has received little focused attention. Some work has been reported for bamboo Cu fibers [56, 57], but the failure mechanism in the present SMAs is likely to differ from that of ductile Cu. In conventional SMAs (non-bamboo structure), fatigue fracture surfaces have been observed to be brittle in Cu-Al-Ni single crystals [52], brittle intergranular in Cu-Al-Ni polycrystals [58] and ductile transgranular in Cu-Al-Be polycrystals [59]. For Cu-Zn-Al polycrystals, brittle intergranular fracture has been reported [14, 15, 26].

In a perfect bamboo structure, we envision that fracture may occur either along a boundary or inside a grain, and for a material like Cu-Zn-Al where brittle intergranular fatigue fracture can be expected, transverse fracture along an individual grain boundary may be anticipated as the dominant mode of fatigue failure. We believe that the removal of most intergranular constraints (i.e., removal of triple junctions) in the oligocrystalline structure should mediate the tendency for fracture in this mode (cf. Fig. 8). On the other hand, deviations from this perfect structure, such as non-perpendicular grain boundaries, errant triple junctions, or small grains not spanning the entire cross section would represent likely weak points for fracture initiation. These possible cases are illustrated schematically in Fig. 9, and combinations of these cases are also possible. Investigation of the fatigued wires revealed two different types of fracture surfaces, the first consistent with a perfect bamboo structure as illustrated in Fig. 9a and b, and the second indicating a deviation from this structure as schematized by Fig. 9c, d and e.

Fig. 10a and b show representative SEM images of the most frequent fracture type in two different wires. Here the fracture surfaces are roughly perpendicular to the wire axis and generally very smooth, suggesting brittle fracture, perhaps along a grain boundary. Some regions with a few dimples characteristic of ductile rupture can also occasionally be observed; these may be associated with the final stages of overload rupture.

Fig. 10c and d present the two matched faces of a single fracture surface that typifies the second type of failure mode. Here the fracture surface is considerably rougher, and also comprises two different fracture planes that adjoin along a line running across the center of the fracture surface. One possible interpretation for this structure is that the line represents a transition from inter- to transgranular crack propagation, as in Fig. 9c. A second interpretation would associate this fracture with a triple junction, as schematized in Fig. 9d, with the two halves of the fracture surface corresponding to two grain boundary planes along which the crack has propagated. This interpretation is supported by the magnified view in Fig. 11 in the vicinity of the apparent triple junction line, which reveals martensite plates in the lower left grain, but not in the other. This is typical for fracture in conventional Cu-based SMAs where stress concentrations arise around triple junctions to maintain coherency between transforming and non-transforming grains, and which can eventually cause fracture along grain boundaries.

While observations of the 11 fatigued wires showed indications consistent with all of the five failure modes in Fig. 9, the majority of cases resembled case a or b, indicating a nearly perfect bamboo grain structure (as expected based on our microstructural observations as in Fig. 1). As the number of samples is relatively small and the number of cycles to failure is around 10^3 for all the samples there is not an unequivocal relation between the mode of failure and fatigue life. However, it is interesting to note that the wire with lowest N_f (sample #8) had a steep angular boundary and failed by intergranular fracture along that boundary as schematized in Fig. 9c.

7. Summary and Conclusions

The structure, transformation behavior, and superelastic characteristics of shape memory alloy microwires with equivalent diameters of 24-114 μm and a bamboo type grain structure were studied experimentally. The results presented here strengthen the argument that the reduction of total grain boundary area relative to the amount of free surface, i.e, the formation of an oligocrystalline structure, dramatically improves the recoverability of shape memory and superelasticity, as well as fatigue lifetime, as compared to bulk polycrystalline Cu-based SMAs. The following specific results of the present study are noteworthy:

- Oligocrystalline Cu-Zn-Al wires tested in tension above A_f exhibit large recoverable strains (up to 7.5%) with little or no residual deformation. When subjected to repeated loading there is a transient shakedown period during which the transformation stresses shift and the hysteresis decreases, but this stabilizes after ~10 cycles. In comparison, conventional polycrystals of the same alloy would exhibit fracture at the first cycle to such strains.
- There is a size effect in energy dissipation in the size range below ~100 μm; smaller diameter fibers damp more energy during a full transformation cycle than larger diameter fibers. Whereas this effect has been reported in Cu-Al-Ni alloys previously, the present observations in Cu-Zn-Al establish the generality of the physics beyond a specific alloy system. Additionally, we find here that the size effect may depend on geometrical details of the wire cross-section, with an apparently better scaling against the smallest sample dimension as opposed to the equivalent diameter.
- Finally, we present the first exploration of fatigue in oligocrystalline SMAs, with a focus on large strains (3-7%), i.e., low-cycle fatigue. The fatigue life of oligocrystalline SMAs is dramatically superior to bulk polycrystalline samples of the same alloy, and comparable to Ni-Ti in the tested strain range. Premature fatigue failure may be associated with defects in the oligocrystalline structure, such as errant triple junctions and unexpected small grains that do not span the cross-section.

Acknowledgments

This work was supported by the US Office of Army Research, through the Institute for Soldier Nanotechnologies at MIT.

[1] Karaman I, Ma J, Noebe RD. Int. Mater. Rev. 2010;55:257.
[2] Kainuma R, Tanaka Y, Himuro Y, Sutou Y, Omori T, Ishida K. Science 2010;327:1488.
[3] Tadaki T, Otsuka K, Shimizu K. Annual Review of Materials Science 1988;18:25.
[4] James RD, Zhang ZY, Muller S. Acta Mater. 2009;57:4332.
[5] Karaca HE, Karaman I, Basaran B, Chumlyakov YJ, Maier HJ. Acta Mater. 2006;54:233.
[6] Kim HY, Ikehara Y, Kim JI, Hosoda H, Miyazaki S. Acta Mater. 2006;54:2419.
[7] Lagoudas DC, Kumar PK. Acta Mater. 2010;58:1618.
[8] Mullner P, Chmielus M, Zhang XX, Witherspoon C, Dunand DC. Nat. Mater. 2009;8:863.
[9] Shabalovskaya S, Anderegg J, Van Humbeeck J. Acta Biomaterialia 2008;4:447.
[10] Sutou Y, Omori T, Yamauchi K, Ono N, Kainuma R, Ishida K. Acta Mater. 2005;53:4121.
[11] V R, Perez-Saez RB, Bocanegra EH, No ML, San Juan J. Metallurgical and Materials Transactions a-Physical Metallurgy and Materials Science 2002;33:2581.
[12] Waitz T, Antretter T, Fischer FD, Simha NK, Karnthaler HP. Journal of the Mechanics and Physics of Solids 2007;55:419.
[13] Saadat S, Salichs J, Noori M, Hou Z, Davoodi H, Bar-On I, Suzuki Y, Masuda A. Smart Materials & Structures 2002;11:218.
[14] Bertolino G, Larochette PA, Castrodeza EM, Mapelli C, Baruj A, Troiani HE. Mater. Lett. 2010;64:1448.
[15] Oshima R, Yoshida N. Journal De Physique 1982;43:803.
[16] Chen Y, Zhang XX, Dunand DC, Schuh CA. Appl. Phys. Lett. 2009;95.
[17] Chen Y, Schuh CA. Acta Materialia 2011;59:537.
[18] Sutou Y, Koeda N, Omori T, Kainuma R, Ishida K. Acta Mater. 2009;57:5759.
[19] Bertolino G, Gruttadauria A, Larochette PA, Castrodeza EM, Baruj A, Troiani HE. Intermetallics 2011;19:577.
[20] Castrodeza EM, Mapelli C, Vedani M, Arnaboldi S, Bassani P, Tuissi A. Journal of Materials Engineering and Performance 2009;18:484.
[21] Dunand DC, Mullner P. Adv. Mater. (Weinheim, Ger.) 2011;23:216.
[22] Juan JMS, No ML, Schuh CA. Advanced Materials 2008;20:272.
[23] Juan JS, No ML, Schuh CA. Nature Nanotechnology 2009;4:415.
[24] Qiao L, Rimoli JJ, Chen Y, Schuh CA, Radovitzky R. Physical Review Letters 2011;106.
[25] Sade M, Rapacioli R, Ahlers M. Acta Metallurgica 1985;33:487.
[26] Melton KN, Mercier O. Materials Science and Engineering 1979;40:81.
[27] Miyazaki S, Mizukoshi K, Ueki T, Sakuma T, Liu YN. Materials Science and Engineering a-Structural Materials Properties Microstructure and Processing 1999;273:658.
[28] Donald IW. J. Mater. Sci. 1987;22:2661.
[29] Taylor GF. Physical Review 1924;23:655.
[30] Saburi T, Inada Y, Nenno S, Hori N. Journal De Physique 1982;43:633.
[31] Chandrasekaran M, Cooreman L, Vanhumbeeck J, Delaey L. Scripta Metallurgica 1989;23:237.
[32] Ono N. Materials Transactions Jim 1990;31:381.
[33] Rogueda C, Vacher P, Lexcellent C, Contardo L, Guenin G. J. Phys. IV 1991;1:409.
[34] Yawny A, Sade M, Eggeler G. Z. Metallkd. 2005;96:608.
[35] Simon T, Kroger A, Somsen C, Dlouhy A, Eggeler G. Acta Mater. 2010;58:1850.
[36] Ibarra A, Caillard D, San Juan J, No ML. Appl. Phys. Lett. 2007;90.
[37] Pons J, Sade M, Lovey FC, Cesari E. Materials Transactions Jim 1993;34:888.
[38] Roqueta DO, Lovey FC, Sade M. Scr. Mater. 1997;36:385.
[39] Lovey FC, Torra V, Isalgue A, Roqueta D, Sade M. Acta Metall. Mater. 1994;42:453.
[40] Miyazaki S, Imai T, Igo Y, Otsuka K. Metallurgical Transactions a-Physical Metallurgy and Materials Science 1986;17:115.
[41] Eggeler G, Hornbogen E, Yawny A, Heckmann A, Wagner M. Materials Science and Engineering a-Structural Materials Properties Microstructure and Processing 2004;378:24.
[42] Kawaguchi M, Ohashi Y, Tobushi H. Jsme International Journal Series I-Solid Mechanics Strength of Materials 1991;34:76.
[43] Soul H, Isalgue A, Yawny A, Torra V, Lovey FC. Smart Materials & Structures 2010;19.

[44] Strnadel B, Ohashi S, Ohtsuka H, Miyazaki S. Materials Science and Engineering a-Structural Materials Properties Microstructure and Processing 1995;203:187.
[45] Ibarra A, San Juan J, Bocanegra EH, No ML. Acta Mater. 2007;55:4789.
[46] Norfleet DM, Sarosi PM, Manchiraju S, Wagner MFX, Uchic MD, Anderson PM, Mills MJ. Acta Mater. 2009;57:3549.
[47] Brofman PJ, Ansell GS. Metallurgical Transactions a-Physical Metallurgy and Materials Science 1983;14:1929.
[48] Hayzelden C, Cantor B. Acta Metallurgica 1986;34:233.
[49] Mukunthan K, Brown LC. Metallurgical Transactions a-Physical Metallurgy and Materials Science 1988;19:2921.
[50] Umemoto M, Owen WS. Metallurgical Transactions 1974;5:2041.
[51] Pons J, Lovey FC, Cesari E. Acta Metallurgica Et Materialia 1990;38:2733.
[52] Sakamoto H. Transactions of the Japan Institute of Metals 1983;24:665.
[53] Siredey-Schwaller N, Eberhardt A, Bastie P. Smart Materials & Structures 2009;18.
[54] Sawaguchi T, Kaustrater G, Yawny A, Wagner M, Eggeler G. Metallurgical and Materials Transactions a-Physical Metallurgy and Materials Science 2003;34A:2847.
[55] Figueiredo AM, Modenesi P, Buono V. International Journal of Fatigue 2009;31:751.
[56] Khatibi G, Betzwar-Kotas A, Groger V, Weiss B. Fatigue & Fracture of Engineering Materials & Structures 2005;28:723.
[57] Yang B, Motz C, Grosinger W, Dehm G. Materials Science and Engineering a-Structural Materials Properties Microstructure and Processing 2009;515:71.
[58] Sakamoto H, Kijima Y, Shimizu K. Transactions of the Japan Institute of Metals 1982;23:585.
[59] Zhang YF, Camilleri JA, Zhu SY. Smart Materials & Structures 2008;17.

Figure 1. (color online) (a) Montaged optical micrograph showing a longitudinal cross section of a Cu-Zn-Al wire with a bamboo grain structure. Martensite plates are observed in many of the grains, spanning the entire cross section of the wire. (b-d) Polished transverse cross sections of typical wires showing a variety of cross-sections. Arrows in (d) illustrate the long and short axes of the wire.

Figure 2. (color online) Thermal cycling data for sample #2 at constant loads of 3 MPa and 17 MPa showing determination of A_f.

Figure 3. (color online) True stress-true strain curves for sample #4 at 50 ºC obtained at increasing applied load levels.

Figure 4. (color online) True stress-true strain curves for sample #10, obtained at different times (different cycle numbers, N) during isothermal mechanical cycling at 30ºC.

Figure 5. (color online) Evolution of energy dissipation with load cycle number, N, normalized by the value measured during the 1st cycle, for 3 wires with different equivalent diameters. The dotted lines are smoothed interpolations and are meant to serve as a guide for the eye.

Figure 6. (color online) Evolution of the absolute energy dissipation with cycle number N for 3 wires with different diameters. These are the same data from Fig. 6, now on an absolute scale.

Figure 7. (color online) The sample size effect on energy dissipation is presented, (a) in terms of the equivalent wire diameter, D, and (b) in terms of the absolute dimension of the short wire axis, for the 1st and 50th superelastic cycle. The dotted lines represent a power-law fit.

Figure 8. (color online) Fatigue life data for SMAs; strain amplitude plotted against number of cycles to failure, N_f, for present microwires, polycrystalline Cu-Zn-Al, single crystalline Cu-Zn-Al, Ni-Ti and Ni-Ti-Cu.

Figure 9. (color online) Schematics of various possible fracture modes in oligocrystalline wires of (a,b) idealized bamboo structure, and (c-e) imperfect, near-bamboo structures. (a) intergranular fracture, (b) transgranular fracture, (c) fracture initiated along an inclined grain boundary, (d) fracture initiated at a triple junction and (e) grain pop-out followed by transgranular fracture.

Figure 10. SEM images of fracture surfaces of fatigued wires showing (a) a smooth, planar fracture of a wire with an equiaxed cross-section, (b) a similar planar fracture in a highly lenticular wire, and (c and d) two complementary images of the mating fracture surfaces where the cross section appears to contain two grains and where the surface is rougher than in (a) and (b).

Figure 11. Higher magnification image of Fig. 10d showing that martensite plates are clearly visible on one face of the fracture surface, but not on the other. This may speak to the presence of a triple junction line in the specimen.

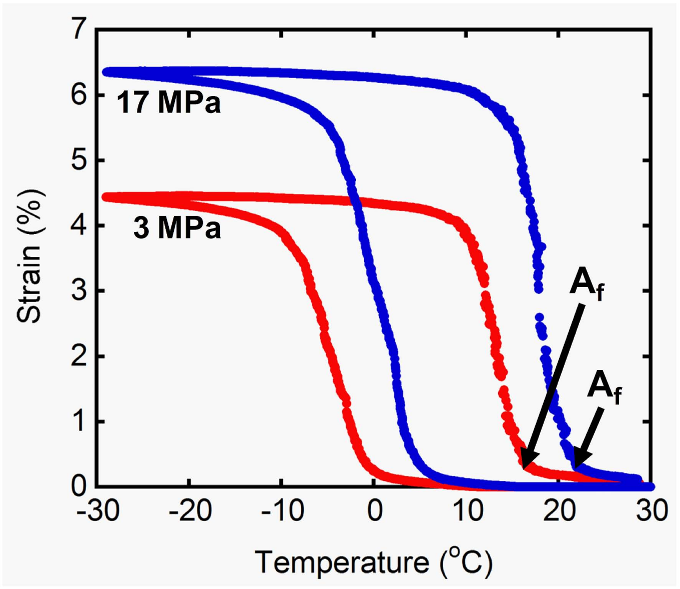

Strain (%)
Temperature (°C)
17 MPa
3 MPa
A_f
A_f
0
1
2
3
4
5
6
7
-30
-20
-10
0
10
20
30

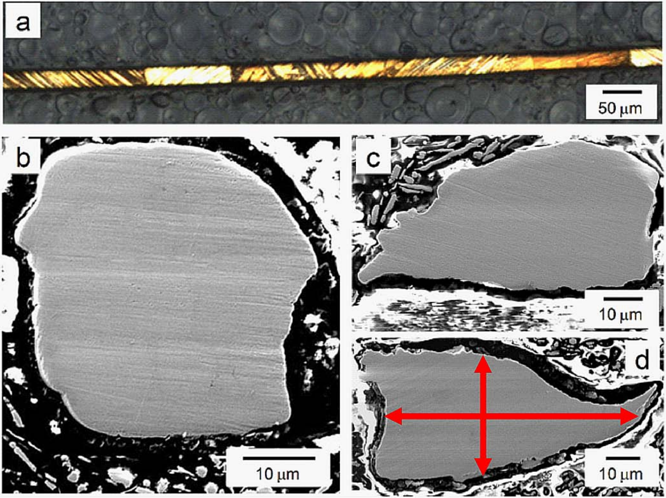
a
50 μm
b
10 μm
c
10 μm
d
10 μm